

# Morphology modulation of SiC nano-additives for mechanical robust high thermoelectric performance $\text{Mg}_2\text{Si}_{1-x}\text{Sn}_x/\text{SiC}$ nano-composites

Kang Yin <sup>a</sup>, Xianli Su <sup>a,\*</sup>, Yonggao Yan <sup>a</sup>, Hao Tang <sup>a</sup>, Mercouri G. Kanatzidis <sup>b</sup>, Ctirad Uher <sup>c</sup>, Xinfeng Tang <sup>a,\*</sup>

<sup>a</sup> State Key Laboratory of Advanced Technology for Materials Synthesis and Processing, Wuhan University of Technology, Wuhan 430070, PR China

<sup>b</sup> Department of Chemistry, Northwestern University, Evanston, IL 60208, USA

<sup>c</sup> Department of Physics, University of Michigan, Ann Arbor, MI 48109, USA

## ARTICLE INFO

### Article history:

Received 29 July 2016

Received in revised form 11 August 2016

Accepted 12 August 2016

Available online xxx

### Keywords:

$\text{Mg}_2\text{Si}_{1-x}\text{Sn}_x$

Nano-composite

Thermoelectric properties

Mechanical properties

## ABSTRACT

SiC nano-powders and nano-wires with excellent toughness as well as high strength were incorporated in  $\text{Mg}_{2.16}(\text{Si}_{0.3}\text{Sn}_{0.7})_{0.98}\text{Sb}_{0.02}$ . The effect of the morphology and phase fraction of nano-SiC additives on the thermoelectric (TE) as well as mechanical properties of the composite was characterized in detail. It is found that, due to the pinning effect, fiber bridging and fiber pull-out mechanisms, the fracture toughness and the compressive strength of the composite with 0.8 at.% SiC nano-powders or nano-wires are improved by about 50% and 30%, respectively. And the TE properties changed little, with a maximum  $ZT$  value of  $\sim 1.20$  at 750 K.

© 2016 Published by Elsevier Ltd on behalf of Acta Materialia Inc.

Thermoelectric (TE) materials, which are capable of generating electrical power owing to the Seebeck effect, are promising as green and clean candidates for waste heat recovery in vehicles and industrial processes. The performance of TE materials is assessed by the dimensionless figure of merit,  $ZT = S^2\sigma T/\kappa_T$ , where  $S$ ,  $\sigma$ ,  $T$ , and  $\kappa_T$  are the Seebeck coefficient, the electrical conductivity, the absolute temperature, and the total thermal conductivity, respectively. Therefore, high power factor ( $S^2\sigma$ ) and low thermal conductivity are essential for developing high performance TE materials.  $\text{Mg}_2\text{Si}_{1-x}\text{Sn}_x$  ( $0 \leq x \leq 1$ ) based solid solutions are a family of materials intended for TE power generation in the temperature range of 300–800 K, with the advantages of good TE performance, as well as inexpensive and environmentally friendly raw materials [1]. The phase composition and the TE performance of  $\text{Mg}_2\text{Si}_{1-x}\text{Sn}_x$  solid solutions depend largely on the Si/Sn ratio, with the compositions near  $x = 0.7$  being particularly promising. As reported recently [2,3], band convergence occurs in  $\text{Mg}_2\text{Si}_{0.3}\text{Sn}_{0.7}$ , whereby the band edges of the light and heavy conduction bands coincide in energy. Such band convergence enhances the number of carrier valleys  $N_v$  participating in the transport process, leading to a significant enhancement of the density-of-states (DOS) effective mass  $m^* = N_v^{2/3}m_b^*$  without increasing the band effective mass  $m_b^*$ . As a result, a sharp increase in the Seebeck coefficient is observed. The band convergence, together with an overstoichiometric content of Mg and suitable Sb or Bi doping, enhances the  $ZT$  value of  $\text{Mg}_2\text{Si}_{0.3}\text{Sn}_{0.7}$  beyond 1.30 at about 750 K [4–6]. Moreover, the most recent studies indicate that a single phase  $\text{Mg}_2\text{Si}_{0.3}\text{Sn}_{0.7}$  will be obtained when heat-

treated at about 1080 K [7], and a long term service life is possible when operated below 823 K in air with BN coatings [8]. Thus, solid solutions based on the  $\text{Mg}_2\text{Si}_{0.3}\text{Sn}_{0.7}$  composition show excellent prospects as n-type legs for TE power generation [7].

However, for viable commercial applications, in addition to excellent TE properties, good mechanical properties are also very important. Usually,  $\text{Mg}_2\text{Si}_{1-x}\text{Sn}_x$  solid solutions fail via the brittle fracture mode [8], i.e., no apparent plastic deformation takes place before fracture and cracks are easily observed due to the thermomechanical stress when working at high temperatures. Hence, it is challenging in the machining processes (like cutting and polishing) when fabricating modules based on  $\text{Mg}_2\text{Si}_{1-x}\text{Sn}_x$  solid solutions. Previous studies found [9,10] that  $\text{Mg}_2\text{Si}_{1-x}\text{Sn}_x$  solid solutions have a reasonable value of the Vickers hardness (3.07–3.54 GPa at room temperature), but showed low fracture toughness ( $\sim 0.48 \text{ MPam}^{1/2}$  at room temperature). Thus, improving the mechanical properties, especially the fracture toughness, is an important task to solve.

It has been shown that incorporating additives with high strength and high elastic modulus is a good way to improve the toughness of composites [11–13]. In this work, we make use of SiC nano-powders and nano-wires in an attempt to improve the mechanical properties of  $\text{Mg}_2\text{Si}_{1-x}\text{Sn}_x$  solid solutions without any notable TE performance degradation. The choice of SiC is obvious. SiC possesses excellent mechanical properties (with a flexural strength of 640 MPa, and a fracture toughness of  $3.8 \text{ MPam}^{1/2}$  at room temperature), low coefficient of thermal expansion ( $2.77 \times 10^{-6} \text{ K}^{-1}$  at room temperature), low density ( $3.21 \text{ gcm}^{-3}$ ), and good thermal stability (melt at 3103 K) [14,15]. The effects of the phase fraction and morphology (i.e. nano-powders vs. nano-wires) of SiC on the thermoelectric and mechanical properties

\* Corresponding authors.

E-mail addresses: [suxianli@whut.edu.cn](mailto:suxianli@whut.edu.cn) (X. Su), [tangxf@whut.edu.cn](mailto:tangxf@whut.edu.cn) (X. Tang).

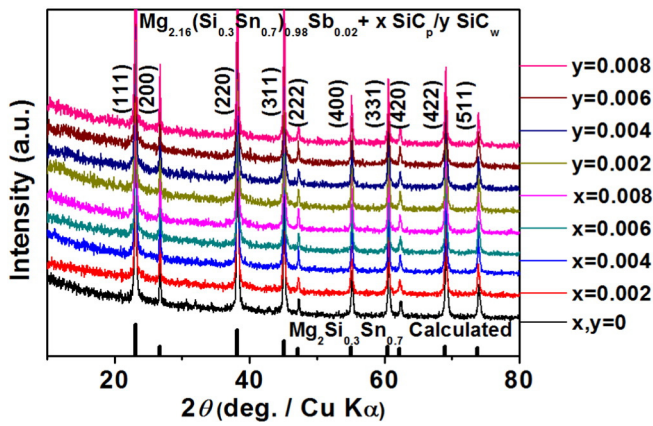


Fig. 1. PXRD patterns of  $\text{Mg}_{2.16}(\text{Si}_{0.3}\text{Sn}_{0.7})_{0.98}\text{Sb}_{0.02}$  with different amounts of SiC nano-powder or nano-wires.

of  $\text{Mg}_{2.16}(\text{Si}_{0.3}\text{Sn}_{0.7})_{0.98}\text{Sb}_{0.02}$  solid solution have been characterized in detail, and significant enhancements in the mechanical properties are observed while maintaining an excellent TE performance.

High purity powders of Mg (99%, 100–200 mesh), Si (99.99%, 200 mesh), Sn (99.9%, 200 mesh), Sb (99.999%, 200 mesh), SiC nano-powders (SiC<sub>p</sub>, 3C-SiC, 99.99%, 40 nm, Aladdin), and SiC nano-wires (SiC<sub>w</sub>, 3C-SiC, 99.9%, prepared by CVD, 0.1–0.6 μm in diameter with the length of 100–500 μm, Changsha Sinet Advanced Materials), were used as starting materials to prepare samples with the nominal composition of  $\text{Mg}_{2.16}(\text{Si}_{0.3}\text{Sn}_{0.7})_{0.98}\text{Sb}_{0.02} + x \text{SiC}_p / y \text{SiC}_w$  ( $x, y = 0, 0.002, 0.004, 0.006, 0.008$ ). A proven two-step solid state reaction method was applied here, with the initiated reaction at 873 K for 24 h and the second reaction at 1080 K for 24 h, samples were placed in the pyrolytic boron nitride (PBN) crucibles and sealed in the silica ampoules during the reactions [16]. The final consolidation into an ingot was done by spark plasma sintering at 930 K for 5 min as described elsewhere. An 8% excess of Mg over the stoichiometry was applied to compensate for the evaporation loss of Mg during the preparation process [6].

The phase composition of the resulting materials was checked on a PANalytical X'Pert Empyrean X-ray diffractometer by Cu K<sub>α</sub> radiation ( $\lambda = 1.5406 \text{ \AA}$ ), within a range of 10–80 degrees and a step size of 0.02 degree. The morphology of the fractured surface was determined by the field-emission scanning electron microscopy (FESEM, Hitachi SU8020) equipped with EDX (XFlash 6160, Bruker). Additionally, for the sample shown in Fig. 2, etching by a 2 vol.% nitric acid ethanol solution for 5–10 s was applied before the FESEM characterization. Transport properties, namely the electrical conductivity  $\sigma$  and the Seebeck coefficient  $S$  in the range of 300–800 K were obtained on a commercial ZEM-3 system (Ulvac Sinku-Riko) operated under helium gas. The Hall coefficient  $R_H$  at 300 K was measured by the five probe method using a physical property measurement system (PPMS, Quantum Design), using a magnetic field of  $\pm 2 \text{ T}$ . The carrier concentration  $n_H$  and the carrier mobility  $\mu_H$  were obtained from the relations  $n_H = 1/(eR_H)$  and  $\mu_H = \sigma R_H$ , respectively, assuming a single parabolic band and acoustic phonon scattering. The total thermal conductivity was determined from  $\kappa_{\text{total}} = \lambda \rho C_p$ , where  $\lambda$  is the thermal diffusivity acquired by the laser flash method (Netzsch LFA 457),  $\rho$  is the density measured by the Archimedes method in alcohol, and  $C_p$  is the specific heat obtained by a differential scanning calorimeter (TA DSC Q20) in argon. The overall errors in measurements of the electrical conductivity, the Seebeck coefficient and the thermal conductivity are estimated to be  $\pm 5\%$ ,  $\pm 3\%$ , and  $\pm 5\%$ , respectively.

Compression tests and three-point flexural tests (the bending span was fixed at 12 mm) were carried out at room temperature using an MTS 810 testing system, with the sample size  $3 \times 3 \times 6 \text{ mm}$  and  $2 \times 2 \times 15 \text{ mm}$ , respectively. 15 samples were prepared for each set of tests [17]. Hardness and fracture toughness was measured on a Vickers indenter (Wilson WH1150), with a load of 1 kg and a dwell time of 15 s. 3 samples were prepared for each set, and 10 indentions were made for each disk-shaped sample of 15 mm diameter and 3 mm thickness. Relevant equations for the calculation of the Vickers hardness  $H_V$  and the fracture toughness  $K_{IC}$  can be found elsewhere [18].

Fig. 1 shows the powder X-ray diffraction patterns of the composites with different amounts of SiC nano-powders and nano-wires, together with the recalculated reference pattern of  $\text{Mg}_2\text{Si}_{0.3}\text{Sn}_{0.7}$  according to

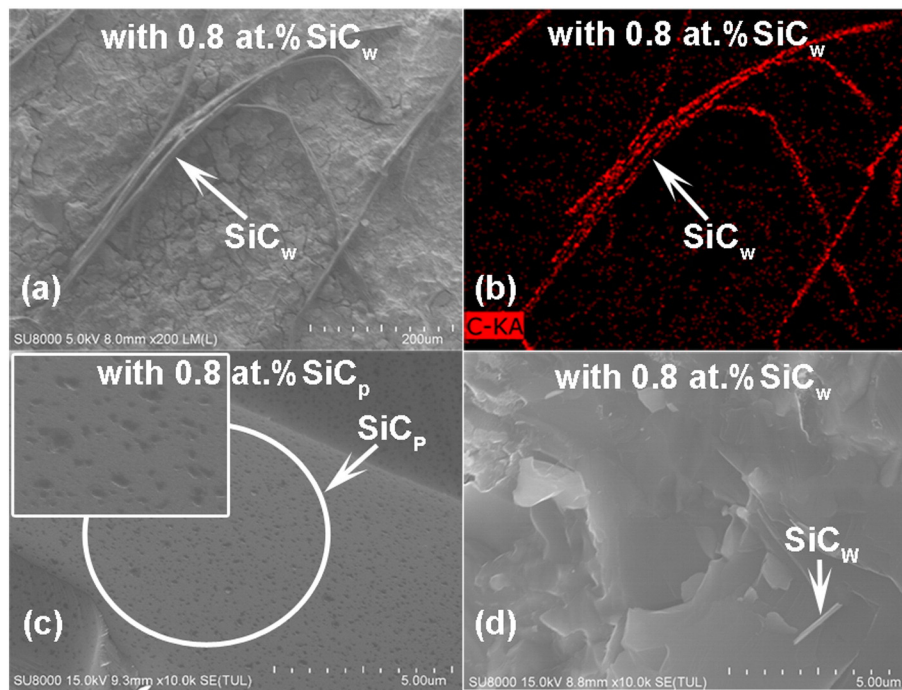


Fig. 2. (a): FESEM images of  $\text{Mg}_{2.16}(\text{Si}_{0.3}\text{Sn}_{0.7})_{0.98}\text{Sb}_{0.02}$  containing 0.8 at.% of SiC nano-wires after metallographic etching; (b): elemental distribution map of SiC nano-wires shown in Fig. 2(a), (c): fracture surface of a composite containing 0.8 at.% of SiC nano-powders, inset: an enlarged view of SiC nano-grains on the grain boundaries of the matrix; (d): fracture surface of a composite containing 0.8 at.% of SiC nano-wires.

Download English Version:

<https://daneshyari.com/en/article/1497989>

Download Persian Version:

<https://daneshyari.com/article/1497989>

[Daneshyari.com](https://daneshyari.com)